Advanced Modulation Strategy for a Three-phase AC-DC Dual Active Bridge For V2G

Nathan D. Weise, Kaushik Basu, Ned Mohan
Department of Electrical and Computer Engineering
University of Minnesota
Minneapolis, Minnesota 55455
Email: weis0315@umn.edu

***Abstract*—The introduction of Plug-in Hybrid Electric Vehicles (PHEV) and Electric Vehicles (EV) into the consumer market provides opportunities and challenges to implement Vehicle-2-Grid (V2G). V2G is a vehicle that can connect to the grid and consume power to charge its battery pack or supply power to the grid. This paper presents research on a novel converter that implements bidirectional power flow between the grid and a vehicles battery pack. The main advantages of this converter are the following: i) soft switching for all switches of the input converter independent of the load, Zero Current Switching (ZCS) ii) The switching of the input converter is simplified i.e four-step commutation is not required for the four quadrant switches of the input side converter iii) The average power flow through the converter is a linear function of the control variable so the control is simple iv) open loop input power factor correction, v) high power density, vi) isolation. The entire topology has been simulated with the proposed modulation method and simulation results confirm the analytical predictions.**

I. Introduction

Depletion of fossil fuels, increasing oil prices, and the reduction of green house gases has spurred multidisciplinary research on alternatives to fuel. This has bolstered research in the areas of wind power, solar power, wave power, and Vehicle-to-grid (V2G).

V2G is where Plug-in Hybrid Electric Vehicles (PHEV) and Electric Vehicles (EV) are connected to the grid and can consume or supply power [1], [2]. The opportunity is available to implement V2G as PHEV's and EV's gain more traction in the consumer market. The available power in PHEV's and EV's can be used as Distributed Generation (DG) and supply power locally to a load [3]. V2G can also be used for peak load shaving, voltage regulation, and reactive power compensation [4].

Several EV charging topologies have been considered and proposed for PHEV's and EV's [5], [6]. The topology in [7], has bidirectional power flow between the traction drive and the battery but lacks bidirectional power flow between the battery and grid. The proposed converter in [8], is a two stage converter with a 3 level NPC converter followed by a bidirectional DC-DC converter. The converter only has single phase input and lacks isolation. In [9], the converter is an inductive charger but lacks bidirectional power flow. The converter in [10], [11] is a contactless inductive charger and provides bidirectional power flow and isolation, but the topology has two stages, AC-DC back to back with an isolated DC-DC converter. A Z-Source Inverter is proposed in [12]. An advantage of the Z-Source Inverter is that it can work in voltage buck or boost mode but it adds passives, L and C, and lacks isolation. The topology in [13] [14] is designed for single-phase only, uses two stages and lacks isolation. Two new converters are proposed in [15]. The converters reuse the motors inductance as the input inductance but lacks isolation and is for only single-phase. The converter in [16] has isolation and 3-ports, one for low voltage loads, but lacks bidirectional power flow between the grid.

The proposed converter in [17] provides a new topology, Fig. 1, for V2G . The topology provides single stage power conversion with bidirectional power flow capability, accepts single-phase or three-phase input, and isolation. The modulation scheme used in [17] employed a complicated closed loop control and achieved partial input power factor correction . The control strategy added considerable amount of line frequency harmonics in the input current. This paper presents a novel modulation scheme for the same topology that overcomes the problems in [17]. The advantages are as follows : 1) single stage power conversion, 2) isolation with high frequency transformer, 3) high power density, 4) voltage matching through adjustment of the transformer turns ratio, 5) accepts single-phase or three-phase, 6) open loop input power factor correction both in single and three-phase, 7) zero current switching (ZCS) in the grid-side converter for all load conditions ensuring high efficiency, 8) bidirectional power flow. The switches in the H-bridge can be reused from the motors inverter.

Section II presents a detailed analysis of the proposed modulation scheme and analytical predictions of important quantities like average power flow, transformer utilization, etc. Section III presents simulations results that confirms the advantages of the proposed scheme.

II. Analysis

This section presents a detailed analysis of the three-phase AC-DC dual active bridge converter, as shown in Fig. 1, with a novel modulation technique proposed in this paper.

The input Converter (A) is a three-phase to single-phase matrix converter supplied by the voltages given in (1). It consists of six four quadrant switches, S_{a1}, S_{b1}, S_{c1}, S_{a2}, S_{b2}, S_{c2}, comprised of two common emitter connected IGBT's. The

978-1-61284-247-9/11/$26.00 ©2011 IEEE

output converter (B) is a H-bridge and consists of IGBT's, S_1, S_2, S_3, S_4.

$$\begin{aligned} v_a(t) &= V_i \cos(\omega_i t) \\ v_b(t) &= V_i \cos\left(\omega_i t - \frac{2\pi}{3}\right) \\ v_c(t) &= V_i \cos\left(\omega_i t - \frac{4\pi}{3}\right) \end{aligned} \tag{1}$$

In this analysis the magnetizing inductance of the transformer is assumed to be very large. The entire leakage inductance of the transformer is lumped into a single inductance $L = L_p n^2 + L_s$. The winding resistances, including both primary and secondary, and also the resistance modeling the core loss is ignored. This transformer is modeled as an ideal transformer with turns ratio $1 : n$ followed by the inductance L in the secondary as in Fig. 1.

Fig. 2 depicts one complete time period of the modulation strategy. In the first third of the period only source v_a and v_b are used. By closing switches S_{a1} and S_{b2} during the first sixth of the period, v_{ab} is applied to the primary. Next $-v_{ab}$ is applied to the primary during the second sixth of the period by closing switches S_{b1} and S_{a2}. During the first third of the time period, the duty ratio d_1, the fraction of time V_d to be applied at v_2 by switching converter B, is given in (2). The duty ratio is chosen such that the average voltage applied across the inductor L over a time period of $T_s/6$ is zero. The voltage applied at v_2 is shown in Fig. 2.

$$\begin{aligned} d_1(t) &= \frac{|v_{ab}(t)|n}{V_d} \\ d_2(t) &= \frac{|v_{bc}(t)|n}{V_d} \\ d_3(t) &= \frac{|v_{ca}(t)|n}{V_d} \end{aligned} \tag{2}$$

The phase shift of the pulse at v_2 with a duration of $\frac{d_1 T_s}{6}$ and amplitude V_d with respect to v_{ab} pulse at v_1 is depicted as Δt in Fig. 2. Δt needs to be restricted so that the pulse of V_d at v_2 is within the time period $\frac{T_s}{6}$. The inequality in (3) imposes this condition. The phase shift δ is defined as a ratio from -1 to 1 as noted in (4). Using the definition (4), (3) can be simplified to (5).

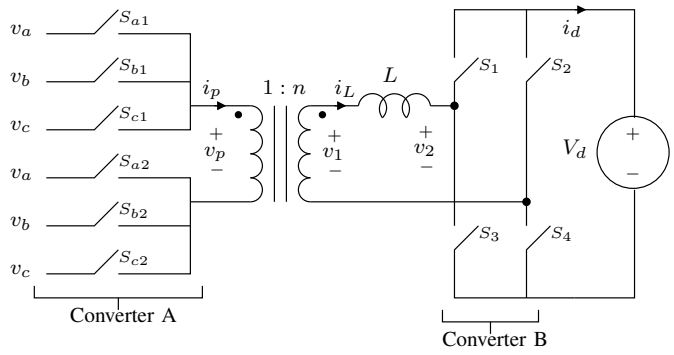

Fig. 1: AC-DC Dual Active Bridge

$$\frac{T_s}{12} + \Delta t + \frac{dT_s}{12} \leq \frac{T_s}{6} \tag{3}$$

$$\delta = \frac{\Delta t}{T_s/12} \tag{4}$$

$$|\delta| \leq 1 - d \tag{5}$$

The voltage across the inductor L is given in (6). It is assumed at the beginning of the cycle T_s, the inductor current is zero. The current reaches I_1 and I_2 at first two consecutive switchings of converter B. At the first switching instant of the converter A the inductor current reaches I_3. Because of the choice of d_1 according to (2) it is expected that I_3 is equal to zero. I_1, I_2, and I_3 are given in (7), (8), and (9). Using (2), (7), (8), and (9) I_3, simplifies to zero. This implies the converter A is switched at zero current (ZCS).

In the second sixth of T_s negative of v_{ab} is applied. In the secondary side of the transformer a V_d pulse of duty ratio d_1, phase shifted by the same amount δ, is applied such that the average voltage applied across the inductor is zero.

$$v_L(t) = n v_p(t) - v_2(t) = L\frac{di_L}{dt} \tag{6}$$

$$I_1 = \frac{n v_{ab}}{L}\left(\frac{T_s}{12} + \Delta t - \frac{dT_s}{12}\right) \tag{7}$$

$$I_2 = I_1 + \frac{n v_{ab} - V_d}{L}\frac{dT_s}{6} \tag{8}$$

$$I_3 = I_2 + \frac{n v_{ab}}{L}\left(\frac{T_s}{12} - \Delta t - \frac{dT_s}{12}\right) \tag{9}$$

$$\langle \bar{i}_{ab} \rangle_{[0-\frac{Ts}{3}]} = \frac{6}{T_s}\int_0^{\frac{T_s}{6}} i_L(t) \tag{10}$$

$$= \frac{n\delta V_d}{4Lf_s} d_1(t) \tag{11}$$

Fig. 3 shows a balanced three-phase star connected source which is actually connected to converter A.

The current i_{ab} is a virtual current depicted in Fig. 3. During the first third of T_s the current i_{ab} is same as i_L. The average i_{ab} current in the first sixth of T_s is the same as the average current in the second sixth of T_s because of the symmetry of the current waveform. Therefore the average current only needs to be calculated during the first sixth of T_s and will be same as the average i_{ab} current during the first third of T_s as given in (10). Given a constant phase shift δ, the average current $\bar{i}_{ab}$ is proportional to the voltage v_{ab}. The virtual current i_{ab} only flows when either switches S_{a1} and S_{b2} are closed or when switches S_{b1} and S_{a2} are closed. This happens only during the first third of T_s consequently the current i_{ab} is zero during the second third and third third of T_s. This results in the average current $\bar{i}_{ab}$ over a full period of T_s being equal to $\frac{1}{3}$ of the average computed in (11). The average current $\bar{i}_{ab}$

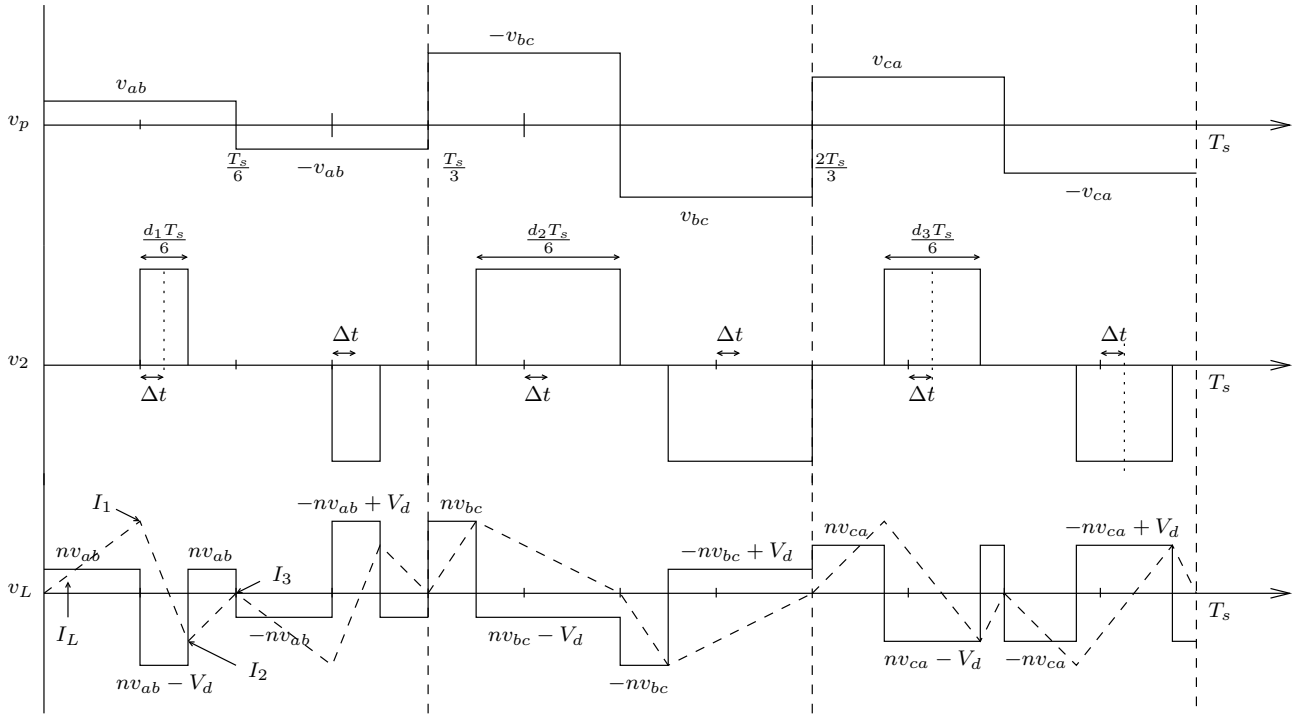

Fig. 2: Modulation Cycle

over a full period of T_s,is given in (12). The analysis for the average current for the first third of T_s is complete.

The average current during the second and third third of T_s is investigated. During the third sixth of T_s, switches S_{b1} and S_{c2} are closed and during the fourth sixth of T_s, switches S_{c1} and S_{b2} are closed. Lastly during the fifth sixth of T_s, switches S_{c1} and S_{a2} are closed and during the sixth sixth of T_s, switches S_{a1} and S_{c2} are closed. The analysis previously shown is repeated for the second third and third third of T_s and leads to the average currents (13) and (14).

$$\bar{i}_{ab} = \frac{\sqrt{3}n^2\delta V_i}{12Lf_s}\cos\left(\omega_i t + \frac{\pi}{6}\right) \tag{12}$$

$$\bar{i}_{bc} = \frac{\sqrt{3}n^2\delta V_i}{12Lf_s}\cos\left(\omega_i t - \frac{\pi}{2}\right) \tag{13}$$

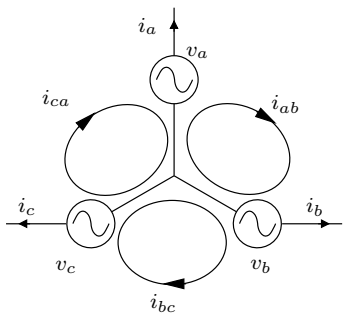

Fig. 3: Virtual Currents

$$\bar{i}_{ca} = \frac{\sqrt{3}n^2\delta V_i}{12Lf_s}\cos\left(\omega_i t - \frac{7\pi}{6}\right) \tag{14}$$

The virtual currents $\bar{i}_{ab}$, $\bar{i}_{bc}$, and $\bar{i}_{ca}$ are shown in Fig. 3. The average currents $\bar{i}_a$, $\bar{i}_b$, $\bar{i}_c$ are calculated using mesh analysis, (15). These currents are shown in (16). Clearly the average currents are sinusoidal and in-phase with the input voltages. This results in unity power factor correction.

$$\begin{aligned}\bar{i}_a &= \bar{i}_{ab} - \bar{i}_{ca}\\ \bar{i}_b &= \bar{i}_{bc} - \bar{i}_{ab}\\ \bar{i}_c &= \bar{i}_{ca} - \bar{i}_{bc}\end{aligned} \tag{15}$$

$$\begin{aligned}\bar{i}_a &= \frac{n^2\delta V_i}{4Lf_s}\cos\left(\omega_i t\right)\\ \bar{i}_b &= \frac{n^2\delta V_i}{4Lf_s}\cos\left(\omega_i t - \frac{2\pi}{3}\right)\\ \bar{i}_c &= \frac{n^2\delta V_i}{4Lf_s}\cos\left(\omega_i t - \frac{4\pi}{3}\right)\end{aligned} \tag{16}$$

The duty cycles in (2) are time varying and they reach their extrema when the corresponding line to line voltages peak. The maximum value of d, defined as $\hat{d}$, is given in (17). As δ remains constant in the entire operation, by (5), the maximum value of $|\delta|$ must be less than or equal to $(1-\hat{d})$. Note that as d is actually a duty ratio, $\hat{d}$ has to be a positive fraction. Given V_i and V_d, the turns ratio n has to be chosen in order to keep $\hat{d}$ within its permissible range.

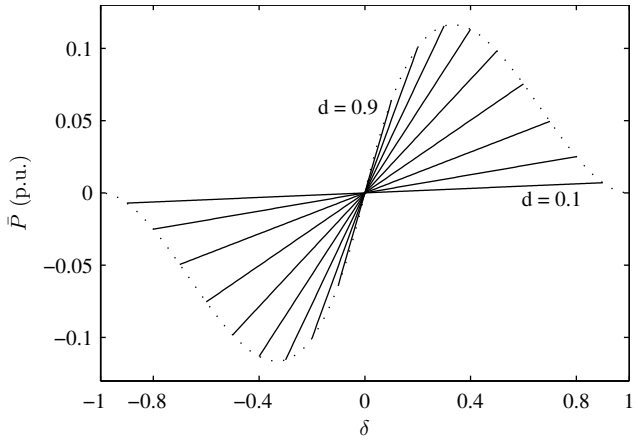

Fig. 4: Average Power Per Unit

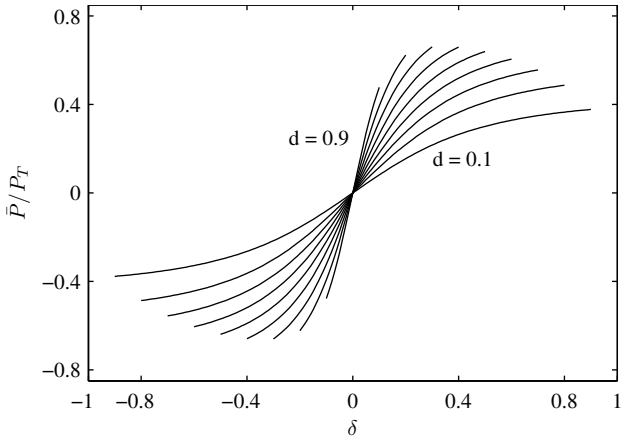

Fig. 5: Transformer Utilization

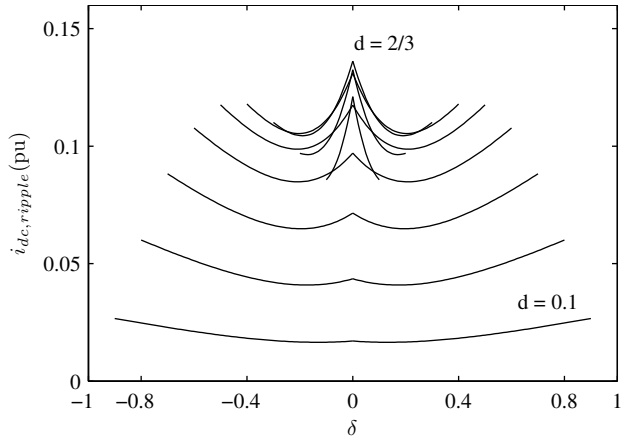

Fig. 6: Output RMS Ripple Current

The average power for this converter can be computed over a cycle of T_s using (16) and (18). As this power is constant, this is also the average power, $\bar{P}$, that flows through this converter over a complete cycle of the input voltages. The average power is converted to per unit using the base (21) and plotted for various fixed values of $\hat{d}$ over the allowable range of δ in Fig. 4.

$$\hat{d} = \frac{n\sqrt{3}V_i}{V_d} \tag{17}$$

$$\langle \bar{P} \rangle_{T_s} = v_a \bar{i}_a + v_b \bar{i}_b + v_c \bar{i}_c \tag{18}$$

$$= \frac{1}{8} \frac{\hat{d}^2 V_d^2}{L f_s} \delta \tag{19}$$

$$= \bar{P} \tag{20}$$

$$P_{base} = \frac{V_d^2}{2\pi f_s L} \tag{21}$$

Note that $\bar{P}_{pu}$ is a linear function of the control variable δ, unlike the classical DAB case, here the control is relatively simple. The maximum $\bar{P}_{pu}$ per unit available in this modulation strategy is $(\frac{\pi}{27})$ and it happens at a $\hat{d}$ of $\frac{2}{3}$ and a δ of $\frac{1}{3}$. One of the important quantities in DAB type of converter is the ratio of the average power to the reactive power. Here the reactive power is defined as (22).

$$P_T = \frac{1}{2}(v_{p_{rms}} i_{p_{rms}} + v_{2rms} i_{Lrms}) \tag{22}$$

This is equivalent to the volt-ampere rating of the transformer. This quantity is a measure of the utilization of this type of converter. For example, even when δ is equal to zero, the net average power transferred is zero, but a non trivial amount flows back and forth between the two sources. This ratio has been plotted as a function of δ for various fixed values of $\hat{d}$ in Fig. 5. An interesting observation in Fig. 5, is that the maximum utilization of the converter occurs at a $\hat{d}$ equals to $\frac{2}{3}$. It is the same $\hat{d}$ that provides the maximum amount of power transfer.

The per unit RMS ripple current ($i_{base} = \frac{V_d}{2\pi f_s L}$) through V_d, which is a measure of the output capacitor size, is plotted for various fixed $\hat{d}$, as a function of δ in Fig. 6. Considering a design just based on the minimum ripple current would lead to a duty ratio of zero or near zero which is undesirable. Upon further investigation of the plots in Fig. 6, it is observed that there is maximum near $\hat{d}$ equal to $\frac{2}{3}$. The trade off is while operating the converter at maximum average power and utilization, the ripple current is also maximum.

To conclude the optimum choice of $\hat{d}$ is $\frac{2}{3}$.

III. Simulation

The converter in Fig. 1 is simulated in MATLAB Simulink using the parameters listed in Table I.

Fig. 7 shows the simulation results of v_1, v_2, and i_L for a complete period of T_s. At each switching of the voltage v_1 in Fig. 7, the current i_L is zero which confirms zero current switching in converter A.

The simulation results of the average input current $\bar{i}_a$ along with v_a and the switch current i_a, are shown in Fig. 8. The input current is sinusoidal and in-phase with the input voltage. This confirms unity input power factor correction. Using the

TABLE I: Simulation Values

L	100uH
V_i	100V
V_d	400V
n	1
f_i	60
f_s	3.33kHz
δ	0.3

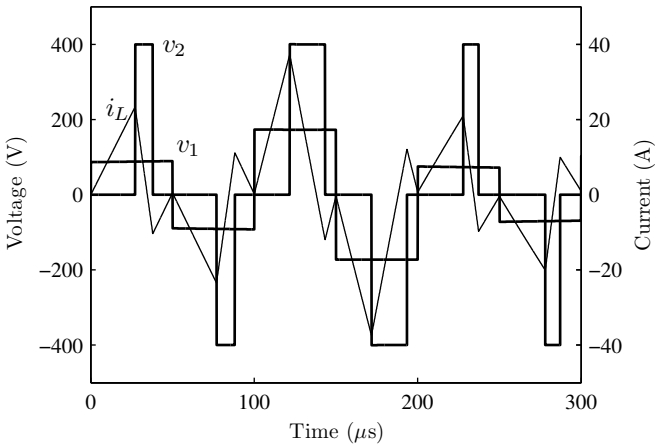

Fig. 7: Simulation Result : Zero Current Switching (ZCS)

values in Table I combined with the equations in (16), the peak of the average currents is 7.5A which matches with the simulation results. Fourier analysis is completed on the input currents i_a, i_b, and i_c. The results are normalized and shown in Fig. 9. The current spectrum contains the fundamental and the switching current at 3.33kHz.

IV. Conclusion

A novel modulation technique for a bidirectional V2G converter has been presented in this paper. The modulation scheme provides open loop sinusoidal input current and through adjustment of phase shift δ the power can be consumed from or

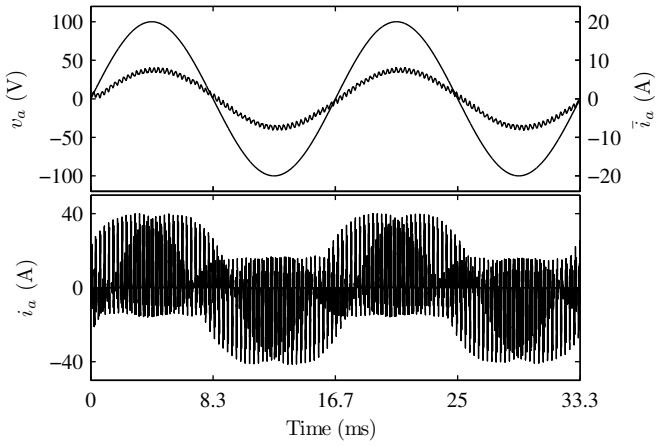

Fig. 8: Simulation Result : Input Power Factor Correction

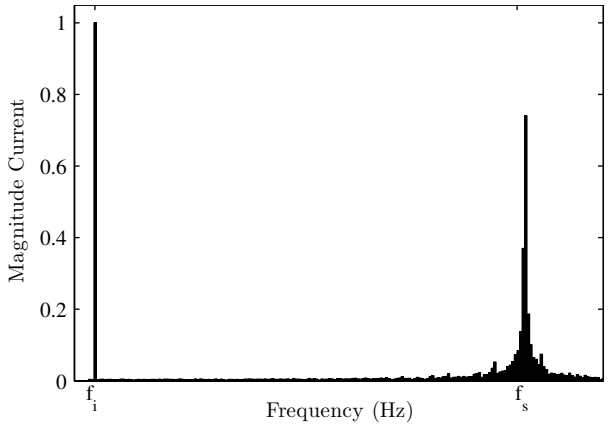

Fig. 9: Frequency Spectrum of i_a

supplied to the grid. The simulation results have confirmed the following advantages: the motor inverter is reused as the h-bridge converter, isolation, bidirectional power flow, open loop input power factor correction, accepts single or three-phase input, zero current switching under all load conditions, single stage converter, voltage matching by design of the transformer turns ratio, and high power density. The topology, with the proposed modulation scheme, presented in this paper provides an integrated, isolated, and bidirectional converter for V2G.

References

[1] J. Tomic and W. Kempton, "Using fleets of electric-drive vehicles for grid support," *Journal of Power Sources*, vol. 168, no. 2, pp. 459–468, 2007.

[2] B. Kramer, S. Chakraborty, and B. Kroposki, "A review of plug-in vehicles and vehicle-to-grid capability," in *Proc. IEEE Industrial Electronics (IECON)*, 2008, pp. 2278 –2283.

[3] M. El Chehaly, O. Saadeh, C. Martinez, and G. Joos, "Advantages and applications of vehicle to grid mode of operation in plug-in hybrid electric vehicles," in *Proc. IEEE Electrical Power Energy Conference (EPEC)*, 2009, pp. 1–6.

[4] M. Kisacikoglu, B. Ozpineci, and L. Tolbert, "Examination of a phev bidirectional charger system for v2g reactive power compensation," in *Proc. IEEE Applied Power Electronics Conference and Exposition (APEC)*, 2010, pp. 458–465.

[5] S. Haghbin, K. Khan, S. Lundmark, M. Alaküla, O. Carlson, M. Leksell, and O. Wallmark, "Integrated chargers for ev's and phev's: examples and new solutions," in *Proc. IEEE International Conference on Electrical Machines (ICEM)*, 2010, pp. 1–6.

[6] D. Erb, O. Onar, and A. Khaligh, "Bi-directional charging topologies for plug-in hybrid electric vehicles," in *Proc. IEEE Applied Power Electronics Conference and Exposition (APEC)*, 2010, pp. 2066–2072.

[7] Y.-J. Lee, A. Khaligh, and A. Emadi, "Advanced integrated bidirectional ac/dc and dc/dc converter for plug-in hybrid electric vehicles," *IEEE Trans. Veh. Technol.*, vol. 58, no. 8, pp. 3970–3980, 2009.

[8] S. Jaganathan and W. Gao, "Battery charging power electronics converter and control for plug-in hybrid electric vehicle," in *Proc. IEEE Vehicle Power and Propulsion Conference (VPPC)*, 2009, pp. 440–447.

[9] M. Egan, D. O'Sullivan, J. Hayes, M. Willers, and C. Henze, "Power-factor-corrected single-stage inductive charger for electric vehicle batteries," *IEEE Trans. Ind. Electron.*, vol. 54, no. 2, pp. 1217–1226, 2007.

[10] U. K. Madawala and D. J. Thrimawithana, "A bi-directional inductive power interface for electric vehicles in v2g systems," *IEEE Trans. Ind. Electron.*, 2011.

[11] D. Thrimawithana, U. Madawala, and Y. Shi, "Design of a bi-directional inverter for a wireless v2g system," in *Proc. IEEE International Conference on Sustainable Energy Technologies (ICSET)*, 2010, pp. 1–5.

[12] O. Ellabban, J. Mierlo, and P. Lataire, "Control of a bidirectional z-source inverter for hybrid electric vehicles in motoring, regenerative braking and grid interface operations," in *Proc. IEEE Electric Power and Energy Conference (EPEC)*, 2010, pp. 1–6.

[13] X. Zhou, S. Lukic, S. Bhattacharya, and A. Huang, "Design and control of grid-connected converter in bi-directional battery charger for plug-in hybrid electric vehicle application," in *Proc. IEEE Vehicle Power and Propulsion Conference (VPPC)*, 2009, pp. 1716–1721.

[14] X. Zhou, G. Wang, S. Lukic, S. Bhattacharya, and A. Huang, "Multi-function bi-directional battery charger for plug-in hybrid electric vehicle application," in *Proc. IEEE Energy Conversion Congress and Exposition (ECCE)*, 2009, pp. 3930–3936.

[15] L. Shi, A. Meintz, and M. Ferdowsi, "Single-phase bidirectional ac-dc converters for plug-in hybrid electric vehicle applications," in *Proc. IEEE Vehicle Power and Propulsion Conference (VPPC)*, 2008, pp. 1–5.

[16] S. Y. Kim, I. Jeong, K. Nam, and H.-S. Song, "Three-port full bridge converter application as a combined charger for phevs," in *Proc. IEEE Vehicle Power and Propulsion Conference (VPPC)*, 2009, pp. 461 –465.

[17] N. Weise, K. Mohapatra, and N. Mohan, "Universal utility interface for plug-in hybrid electric vehicles with vehicle-to-grid functionality," in *Proc. IEEE Power and Energy Society General Meeting*, 2010, pp. 1–8.